Supporting Information

Microstructure and transport modulation in Zn(Al)O-containing $Bi_2Te_{2.7}Se_{0.3}$ films

Yen-Ling Wang, Chuan-Wen Wang, Yu-Chieh Shih, Karan Giri, Yi-Ting Wu, Shin-Syuan Huang, Chun-Hua Chen∗

Department of Materials Science and Engineering, National Yang Ming Chiao Tung University, 1001 Ta-Hsueh Rd., Hsin-Chu, 30010 Taiwan, ROC.
E-mail: ChunHuaChen@nycu.edu.tw, ChunHuaChen@mail.nctu.edu.tw

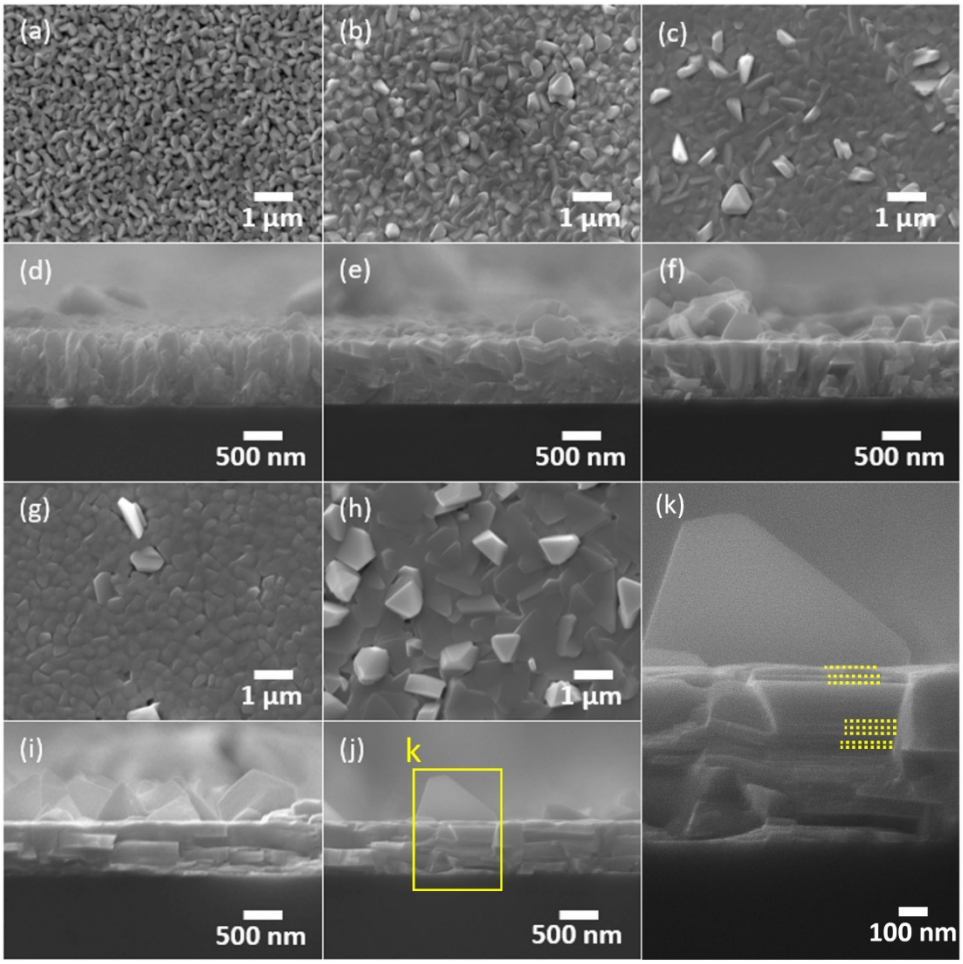

Figure S1. Top-view and cross-sectional SEM images of BTS films deposited at (a, d) 250 °C, (b, e) 300 °C, (c, f) 350 °C, (g, i) 400 °C, and (h, j) 450 °C. (k) Close-up image showing the periodic layered structure of the BTS:AZO films.

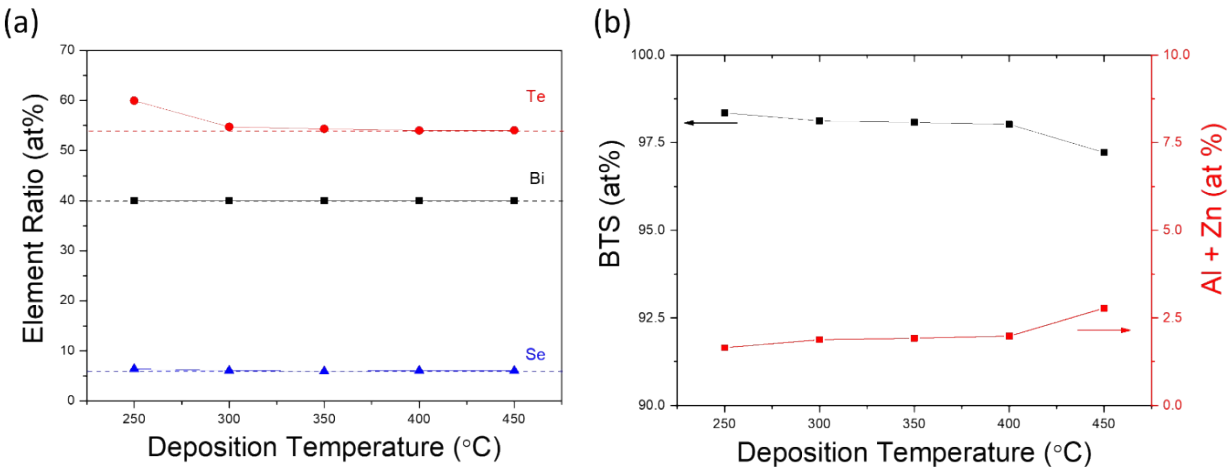

Figure S2. (a) Normalized composition ratios of Bi, Te, and Se, and (b) (b) Normalized atomic fractions of the BTS-related elements (Bi + Te + Se) and (Al + Zn) as a function of deposition temperature..

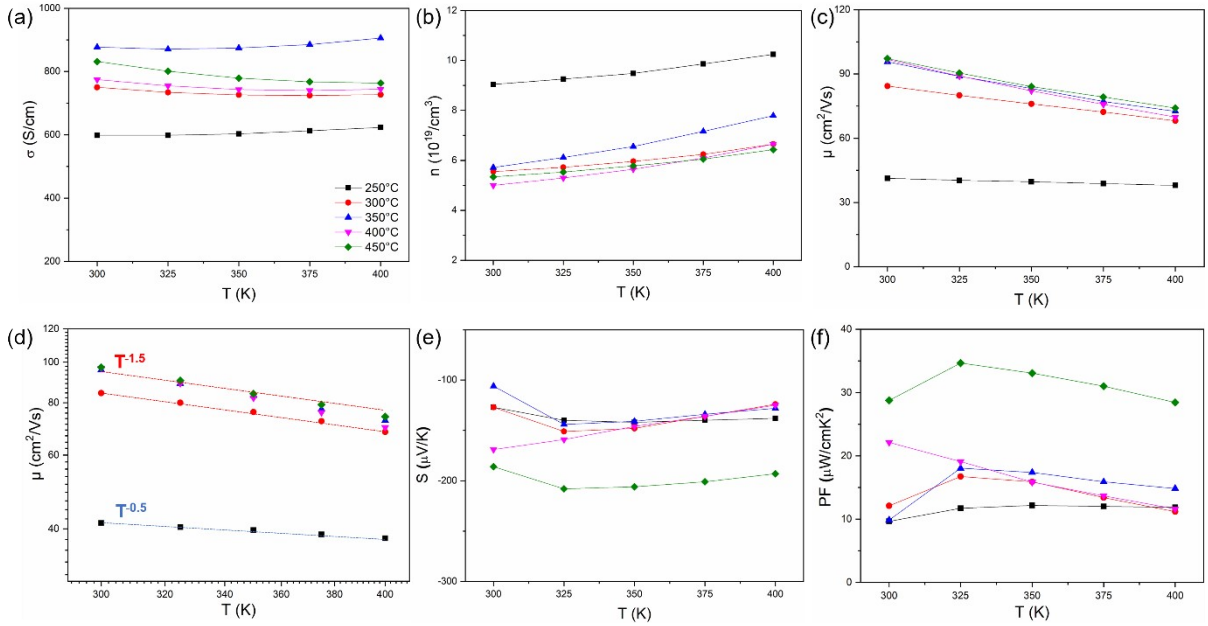

Figure S3. Temperature dependence of (a) electrical conductivity, (b) carrier concentration, (c) carrier mobility, (d) Log-log plot of mobility versus temperature, (e) Seebeck coefficient, and (f) power factor (PF) of the BTS films.

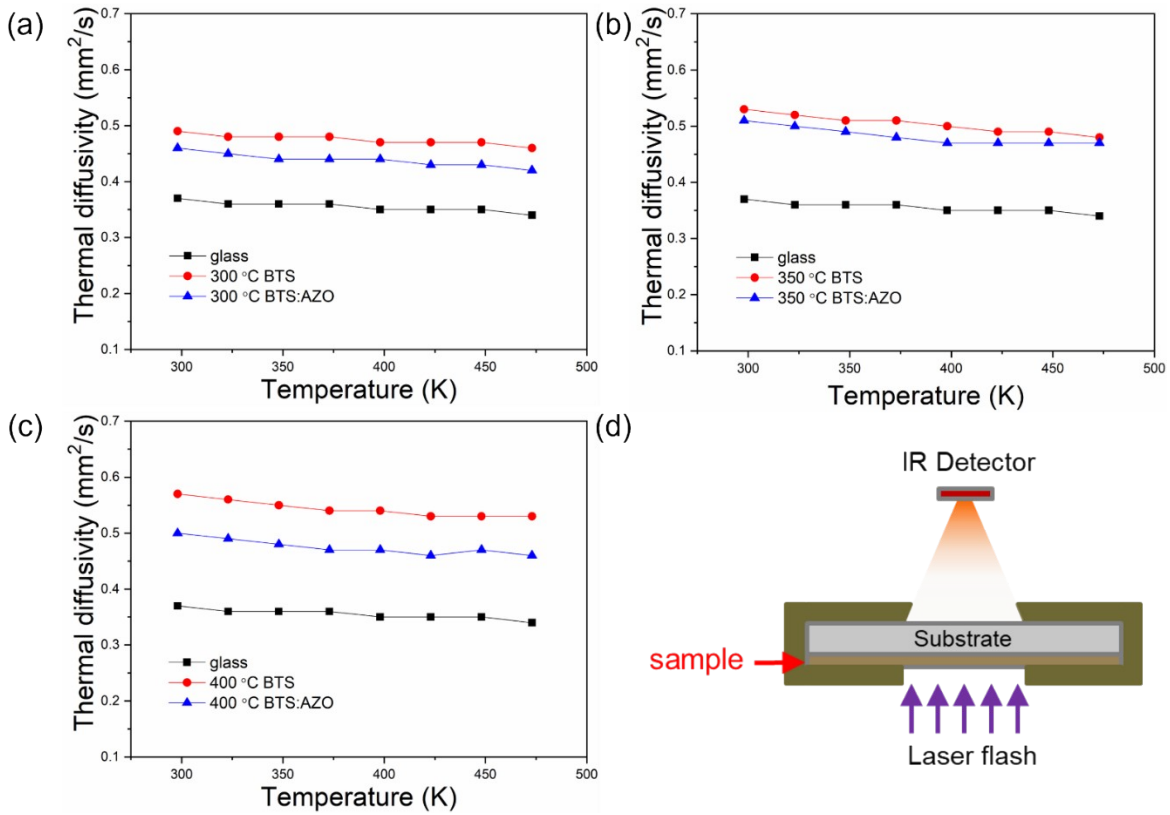

Figure S4. Thermal diffusion coefficients of the glass substrate, BTS, and BTS:AZO films deposited at (a) 300 °C, (b) 350 °C, and (c) 400 °C. (d) Schematic diagram of the thermal diffusion measurement setup.

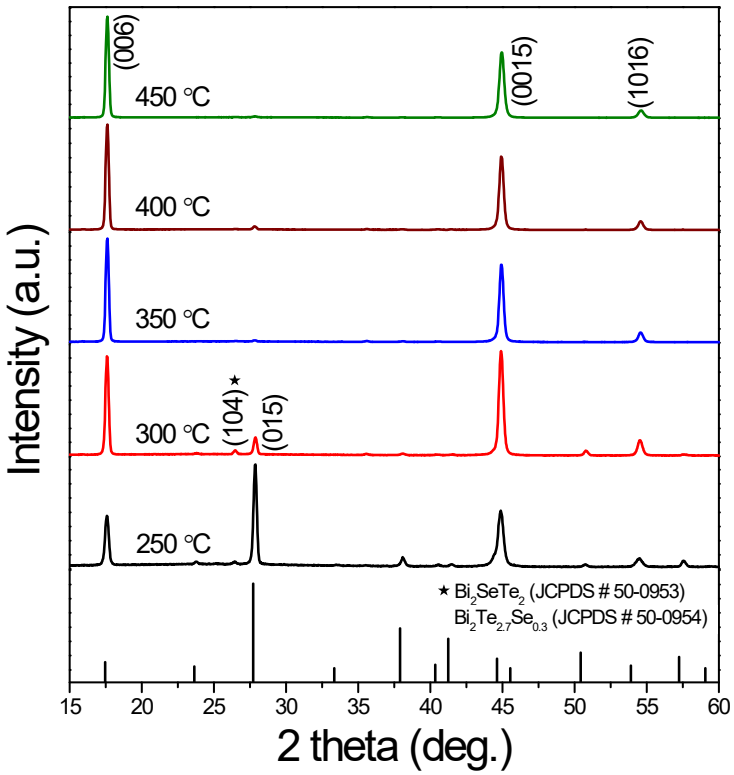

Figure S5. XRD patterns of the BTS films deposited at various temperatures.

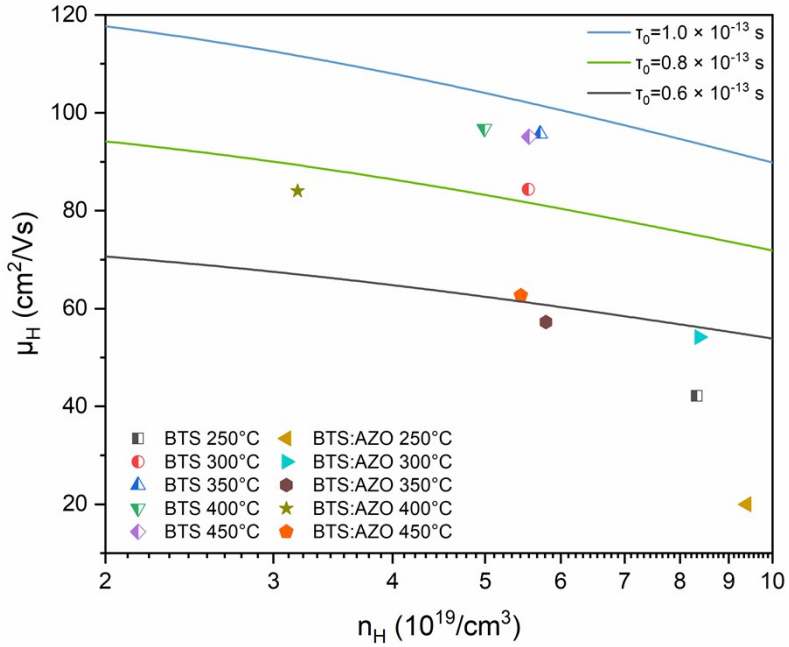

Figure S6. Carrier-density dependent carrier mobility at 300 K.

The carrier mobility (μ) depends on the conductive effective mass m_c^* and the average relaxation time (τ), which can be demonstrated by the following equations when acoustic phonon scattering dominates. Here, constant τ_0 is a n_H-independent relaxation time, and F_0 and $F_{1/2}$ are the Fermi integrals [1].

$$\mu = \frac{e(\tau)}{m_c^*} = \frac{2e\tau_0}{3m_c^*}\frac{F_0}{F_{1/2}} \quad \text{(Eq. 1)}$$

The BTS:AZO films exhibit a relatively lower relaxation time (τ_0), suggesting more frequent carrier scattering. This result is likely due to the various defects introduced by the AZO doping, which increase the scattering events.

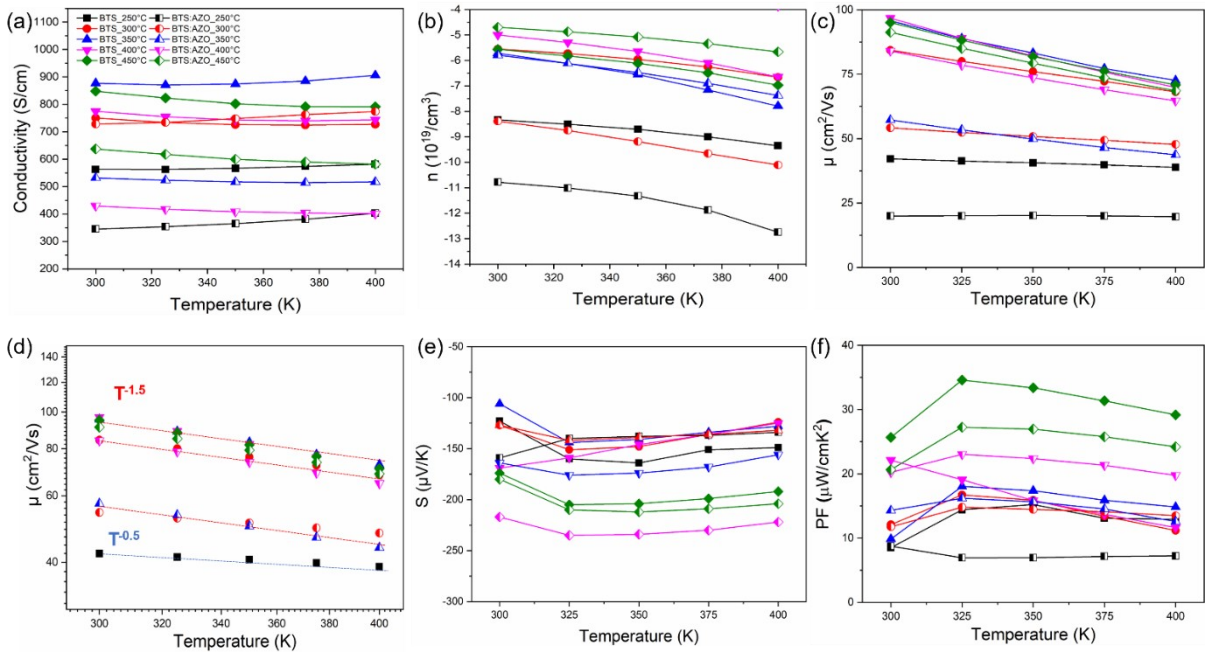

Figure S7. Temperature dependence of the (a) electrical conductivity, (b) carrier concentration, (c) carrier mobility, (d) mobility as a function of T^{-1}, (e) Seebeck coefficient, and (f) PF of the BTS and BTS:AZO films.

Table S1. Composition ratios of Bi, Te, and Se, and AZO doping concentrations in the BTS:AZO films deposited at various deposition temperatures.

BTS:AZO	at%			
	Bi	Te	Se	Te/Bi
250 ℃	37.56	56.29	6.15	1.5
300 ℃	39.67	54.32	6.01	1.48
350 ℃	39.88	54.18	5.94	1.35
400 ℃	39.97	53.97	6.06	1.35
450 ℃	39.95	54.01	6.04	1.35
BTS:AZO	at%			
	Al	Zn	BTS	
250 ℃	0.54	1.11	98.35	
300 ℃	1.00	0.88	98.12	
350 ℃	0.84	1.08	98.08	
400 ℃	1.13	0.85	98.02	
450 ℃	1.06	1.72	97.22	

Table S2. Lattice constants of the BTS and BTS:AZO films deposited at various temperatures.

Sample	BTS		BTS:AZO	
	a=b (Å)	c (Å)	a=b (Å)	c (Å)
250 °C	4.36	30.25	4.36	30.27
300 °C	4.36	30.25	4.35	30.29
350 °C	4.36	30.21	4.36	30.24
400 °C	4.36	30.21	4.36	30.26
450 °C	4.37	30.20	4.35	30.23

Table S3. The full width at half maximum of the (006) diffraction peak and the grain size of the BTS and BTS:AZO films.

Sample	BTS		BTS:AZO	
	FWHM (°)	Grain size (nm)	FWHM (°)	Grain size (nm)
250 °C	0.286	29.1	0.271	30.7
300 °C	0.254	32.8	0.308	27.1
350 °C	0.246	33.9	0.258	32.4
400 °C	0.246	33.9	0.256	32.6
450 °C	0.249	33.5	0.249	33.5

Table S4. Thickness comparison between the BTS and BTS:AZO films

TD (°C)	Sample	Thickness
250	BTS	1153
	BTS:AZO	1003
300	BTS	890
	BTS:AZO	880
350	BTS	827
	BTS:AZO	773
400	BTS	789
	BTS:AZO	753
450	BTS	741
	BTS:AZO	719

Table S5. Comparison of the thermoelectric properties of $Bi_2Te_{2.7}Se_{0.3}$-based films with different compositions and modifications.

Composition	S (μV/K)	PF (μW/cmK^2)	κ (W/mK)	zT	Year, Ref
$Bi_2Te_{2.7}Se_{0.3}$	-180	12	-	-	2010 [2]
$Pt_{0.060}/Bi_2Te_{2.7}Se_{0.3}$	-200	35	0.86	1.17	2014 [3]
$Bi_2Te_{2.7}Se_{0.3}$	-190	18	0.65	0.9	2017 [4]
$Bi_2Te_{2.7}Se_{0.3}$	-240	45	-	1.6	2019 [5]
BTS-2Cu/Ni	-200	29.8	0.93	0.97	2020 [6]
Bi_2Te_3/Te	-160	14.6	-	-	2021 [7]
Bi_2Te_3	-180	47	-	-	2021 [8]
$(CuI)_{0.002}Bi_2Te_{2.7}Se_{0.3}$	-180	63.5	1.5	1.42	2022 [9]
ZnO/BTS	-210	33.5	0.81	1.25	2024 [10]
$Bi_2Te_{2.7}Se_{0.3}$	-155	35.1	1.01	1.14	2026 [11]

References

[1] H. Lee, Thermoelectrics: design and materials, John Wiley & Sons 2025.

[2] X. Duan, Y. Jiang, Applied surface science, 256 (2010) 7365-7370.

[3] T. Sun, M.K. Samani, N. Khosravian, K.M. Ang, Q. Yan, B.K. Tay, H.H. Hng, Nano Energy, 8 (2014) 223-230.

[4] S.J. Kim, H. Choi, Y. Kim, J.H. We, J.S. Shin, H.E. Lee, M.-W. Oh, K.J. Lee, B.J. Cho, Nano Energy, 31 (2017) 258-263.

[5] M. Tan, W.D. Liu, X.L. Shi, H. Gao, H. Li, C. Li, X.B. Liu, Y. Deng, Z.G. Chen, Small Methods, 3 (2019) 1900582.

[6] Y. Wudil, M. Gondal, S. Rao, S. Kunwar, A. Alsayoud, Materials Chemistry and Physics, 253 (2020) 123321.

[7] D.W. Ao, W.D. Liu, Y.X. Chen, M. Wei, B. Jabar, F. Li, X.L. Shi, Z.H. Zheng, G.X. Liang, X.H. Zhang, P. Fan, Z.G. Chen, Advanced Science, 9 (2022) 2103547.

[8] M. Zhang, W. Liu, C. Zhang, S. Xie, Z. Li, F.Q. Hua, J.F. Luo, Z.H. Wang, W. Wang, F. Yan, Y. Cao, Y. Liu, Z.Y. Wang, C. Uher, X.F. Tang, Acs Nano, 15 (2021) 5706-5714.

[9] C.L. Chen, T.H. Wang, Z.G. Yu, Y. Hutabalian, R.K. Vankayala, C.C. Chen, W.P. Hsieh, H.T. Jeng, D.H. Wei, Y.Y. Chen, Advanced Science, 9 (2022) 2201353.

[10] Q. Hu, J. Guo, X. Zhao, C. Guan, S. Wang, Z. Zhao, J Alloy Compd, 1004 (2024) 175770.

[11] Y. Xiong, Y. Shi, G. Dong, T. Wang, X. Chen, S. Zhou, E. Min, J. Feng, J. Li, R. Liu, Journal of Materials Science & Technology, 252 (2026) 48–56.